• 新型纳米材料与器件 •

原子层沉积 MgO 薄膜改性 $LiNi_{0.6}Co_{0.2}Mn_{0.2}O_2$

寇华日[1,3]，李喜飞[1,2*]，刘 文[1,2]，鄯 慧[1,2]，颜 波[1,2]，丁书江[3,4*]

(1. 天津师范大学物理与材料学院 天津 西青区 300387；2. 西安理工大学先进能源与器件中心 西安 710048；
3. 西安交通大学深圳研究院 广东 深圳 518057；4. 西安交通大学理学院 西安 710049)

【摘要】$LiNi_{0.6}Co_{0.2}Mn_{0.2}O_2$ 锂离子电池正极材料由于其较高的能量密度和容量密度获得了广泛的关注。但是这一材料在较高的截止电压下，循环寿命难以令人满意。针对这一问题，该文提出了利用原子层沉积的方法在其表面包覆氧化镁薄膜以改善其高电压下的循环稳定性。研究表明，在 4.5 V 和 4.7 V 的截止电压下，该材料的循环性能和倍率性能均获得了较大的提高。相比于原始材料，经过 100 个循环，在 4.7 V 的截止电压下，改性后的材料的容量仍可达到 158 $mAh \cdot g^{-1}$。

关 键 词 原子层沉积； 氧化镁薄膜； 锂离子电池正极材料
中图分类号 TB321 文献标志码 A doi:10.12178/1001-0548.2020015

Atomic Layer Deposition of Ultrathin MgO Coating onto $LiNi_{0.6}Co_{0.2}Mn_{0.2}O_2$

KOU Hua-ri[1,3], LI Xi-fei[1,2*], LIU Wen[1,2], SHAN Hui[1,2], YAN Bo[1,2], and DING Shu-jiang[3,4*]

(1. College of Physics and Materials Science, Tianjin Normal University Xiqing Tianjin 300387; 2. Center for Advanced Energy Materials and Devices, Xi'an University of Technology Xi'an 710048; 3. Shenzhen Research School, Xi'an Jiaotong University Shenzhen Guangdong 518057; 4. School of Science, Xi'an Jiaotong University Xi'an 710049)

Abstract As one of the most promising cathode materials for high energy density lithium ion batteries, $LiNi_{0.6}Co_{0.2}Mn_{0.2}O_2$ with high reversible capacity suffers poor cycling performances, especially at high cutoff potentials. To address this challenge, in this study, an atomic layer deposition is utilized to design controllable MgO coating layers onto $LiNi_{0.6}Co_{0.2}Mn_{0.2}O_2$ cathode material. It is confirmed that the optimized $LiNi_{0.6}Co_{0.2}Mn_{0.2}O_2$ cathode shows an improved electrochemical performance comparing with the pristine material at the cutoff potentials of 4.5 V as well as 4.7 V. After 100 cycles, the $LiNi_{0.6}Co_{0.2}Mn_{0.2}O_2$ with MgO coating displays the reversible capacities of 157 $mAh \cdot g^{-1}$ and 158 $mAh \cdot g^{-1}$ at the cutoff potential of 4.5 V and 4.7 V, respectively, which is higher than those of the pristine one (131 $mAh \cdot g^{-1}$ and 144 $mAh \cdot g^{-1}$). This study demonstrates that the ALD derived MgO coating layer shows some promising potentials to improve $LiNi_{0.6}Co_{0.2}Mn_{0.2}O_2$ performance for lithium ion batteries. This is mainly due to the effective protection of MgO layer to the material surface, that is, the MgO coating can stabilize the interface and block the metal ion dissolution by reducing the direct connection between $LiNi_{0.6}Co_{0.2}Mn_{0.2}O_2$ and electrolyte.

Key words atomic layer deposition; MgO film; lithium ion battery cathode material

A lithium ion battery system has been known as one of the most promising energy storage devices to address the energy crisis owing to its high energy density, high voltage and long cycling life. For the applications of electric vehicles (EVs) and plug-in hybrid electric vehicles (HEVs), lithium ion batteries (LIBs) are required with high reversible capacities at high cutoff potentials and good cycling stabilities.

Received date: 2019 − 12 − 01; Revised date: 2020 − 01 − 06
收稿日期：2019 − 12 − 01；修回日期：2020 − 01 − 06
Foundation item: National Natural Science Foundation of China (51572194)
基金项目：国家自然科学基金 (51572194)
Biography: KOU Hua-ri was born in 1992, male, his research interests include design and application of lithium and sodium ion battery material interface.
作者简介：寇华日 (1992 −)，男，主要从事锂钠离子电池材料界面设计及应用等方面的研究.
Corresponding author: LI Xi-fei, E-mail: xfli2011@hotmail.com; DING Shu-jiamg, E-mail: dingsj@mail.xjtu.edu.cn
通信作者：李喜飞，E-mail：xfli2011@hotmail.com; 丁书江，E-mail：dingsj@mail.xjtu.edu.cn

Currently, the commercial $LiCoO_2$ cathode may not satisfy the requirements of EVs and HEVs. Because of integrating the advantages of $LiCoO_2$, $LiNiO_2$ and $LiMnO_2$, the $LiNi_xCo_yMn_{1-x-y}O_2$ cathode material has been an available candidate to build high performance LIBs.

To promote the lithium ion storage performance of $LiNi_{1-x-y}Co_xMn_yO_2$, many kinds of $LiNi_{1-x-y}Co_xMn_yO_2$ materials with different ratios of Ni, Co and Mn have been studied[1-4]. As a type of nickel-rich $LiNi_xCo_yMn_{1-x-y}O_2$ (x>0.5) materials, $LiNi_{0.6}Co_{0.2}Mn_{0.2}O_2$ has attracted a lot of attention for its high reversible capacity. However, the dissolution of Ni, Co and Mn ions into the electrolyte occurs upon cycling, causing severe structural damages and degradations of the material stabilities[5-9]. Furthermore, it was demonstrated in a number of studies[10-12] that a high cutoff potential can lead to a high energy density, but an aggravating dissolution of active ions, especially at potentials above 4.3 V.

To address these challenges, a modification of $LiNi_xCo_yMn_{1-x-y}O_2$ cathode is demanded. And a great deal of strategies have been tried to improve the properties of $LiNi_xCo_yMn_{1-x-y}O_2$ cathodes, such as ion doping[13-17], surface coating[1, 4, 18-19], surface reconstruction[20-22], size and shape control[23-25]. Among these methods, surface coating with metal oxides has been verified to be efficient in improving the cathode electrochemical performances, such as Al_2O_3[26-30], MgO[31-35], TiO_2[36-38] and ZnO[39-41]. Due to the hexagonal structure of MgO, a MgO coating layer has negligible effect on Li ion transition[35]. Moreover, the Mg^{2+} ions can diffuse into the interslab space under the pillaring effect with enhancing the structural stability[42-44]. As a result, the MgO coating shows unique advantages comparing with the other metal oxides. To promote the performances of $LiNi_{0.6}Co_{0.2}Mn_{0.2}O_2$ cathodes, moreover, it is essential to obtain a conformal and ultrathin MgO coating layer. But it is of difficulty for the traditional methods, such as sol-gel and wet chemical methods, to produce an ultrathin layer onto the $LiNi_{0.6}Co_{0.2}Mn_{0.2}O_2$. Therefore, how to design an ultrathin MgO coating onto $LiNi_{0.6}Co_{0.2}Mn_{0.2}O_2$ has still been challenging.

Fortunately, an atomic layer deposition (ALD) as an advanced coating method can conveniently synthesize ultrathin films on many kinds of materials[45-49]. The thicknesses of coating layers can be precisely controlled by regulating numbers of deposition reactions. Moreover, our previous results indicated that the electrode modification can well maintain the conductivity network, differing from the powder coating[28, 50]. Interestingly, the whole electrode modification is easy to conduct via ALD, which is challenging for the traditional methods.

In this work, $LiNi_{0.6}Co_{0.2}Mn_{0.2}O_2$ cathodes coated with ultrathin MgO layer were successfully designed. Remarkably, the electrochemical performances of $LiNi_{0.6}Co_{0.2}Mn_{0.2}O_2$ were much improved due to the effective protection of MgO coating from the electrolyte.

1 Experimental

1.1 Material Synthesis

All the reagents were used with no further purification. A mixture of commercial $LiNi_{0.6}Co_{0.2}Mn_{0.2}O_2$, acetylene black and Polyvinylidene Fluoride (PVDF) were well mixed in appropriate amount of 1-Methyl-2-pyrrolidinone (NMP) at a mass ratio of 8:1:1. The resultant slurry was spread on the aluminum foil and dried in a coven at 80 °C for overnight, and the cathode electrodes were obtained. The direct deposition of MgO onto the cathode electrodes was conducted via ALD R200 Advanced system (Picosun, Finland). In the ALD process of MgO, Bis-clopentadienyl magnesium (MSDS) and H_2O were used as the precursor of Mg and oxidizer, respectively. The deposition temperature was set at 200 °C. A typical cycle of MgO deposition was conducted with the following steps: 1) pulsing the MSDS into the reactor for 1.6 s; 2) evacuating the excess MSDS for 5 s; 3) pulsing the H_2O into the reactor for 0.1 s; 4) evacuating the excess H_2O and by product for 8 s. The cathode electrodes with different thicknesses of MgO coating layers were acquired by depositing for 2, 5 and 10 ALD cycles, which were marked as NCM-2c, NCM-5c and NCM-10c, respectively. For comparison, the pristine $LiNi_{0.6}Co_{0.2}Mn_{0.2}O_2$ electrode was noted

as NCM-0c.

1.2 Physical Characterization

NCM-0c and NCM-10c were characterized by X-ray diffraction (XRD, D8 Advance of Bruker, Germany) with Cu-K_α radiation to obtain the crystallinity phases between scattering angles (2θ) of 10°～ 80° at a scanning rate of 10° min^{-1}. The morphologies of the samples were observed by the scanning electron microscopy (SEM, SU8010, Hitachi) and high-resolution transmission electron microscopy (HRTEM, TecnaiG^2 F30, FEI), and the elemental mapping was acquired by SEM (SU8010, Hitachi) with EDAX. The particle size distribution of NCM-0c was obtained via laser particle sizer (Mastersizer 3000, Malvern). The elemental information of the NCM-10c electrode was collected by X-ray photoelectron spectroscopy (XPS, VG ESCALAB MK II).

1.3 Electrochemical Performance

The electrodes obtained were used as working electrodes, and the lithium metal slices acted as both counter and reference electrodes. The electrolyte used in the cells contains 1 M $LiPF_6$ in an ethylene carbonate (EC) and dimethyl carbonate (DMC) mixture (1:1 in volume). The cells were assembled in a glove box with moisture and oxygen contents less than 0.1 ppm. The galvanostatical tests were conducted on a Land battery tester (LANHE CT2001A) using CR2032-type coin cells with the potential ranges of 2.7～4.5 V and 2.7～4.7 V. Cyclic voltammogram (CV) measurements were performed using Princeton Applied Research VersaSTAT4 in the voltage range of 2.7～4.5 V (*vs.* Li/Li^+) at a scan rate of 0.1 $mV \cdot s^{-1}$. Electrochemical impedance spectroscopy (EIS) was also carried out on Princeton Applied Research VersaSTAT4 at an amplitude of 5 mV over the frequency range from 100 kHz to 0.01 Hz. All the electrochemical experiments were conducted at room temperature.

2 Results and Discussion

The typical SEM images of NCM-0c, NCM-2c, NCM-5c and NCM-10c are shown in Fig. 1. As seen in the Fig. 1a, the NCM-0c is combined by primary particles with relatively smooth surface. The NCM-2c, NCM-5c and NCM-10c show uniform MgO coating layers on the surface. Even on the surface of NCM-2c, the dense coating layer may be discerned. And it can also be observed that the amount of MgO increases with increasing ALD cycles. As shown in Fig. 1b～d, the MgO films are compact and conformal which is the outstanding advantage of ALD derived coatings. This kind of ultrathin film can provide a perfect protection for the $LiNi_{0.6}Co_{0.2}Mn_{0.2}O_2$ material. The HRTEM image (Fig. 1e) of NCM-10c displays a thin MgO layer with the thickness of about 3 nm. The low crystallization of conformal-coating layer in Fig. 1e may own to the low conducting temperature[51]. The size distribution curve in Fig. 1f indicates that the particle diameter of NCM-0c is about 10 μm. The distributions of Ni, Co, Mn, O, Mg, F, C are well coincided in the images. It verifies that the MgO film is successfully deposited on the electrode slice. And in the Energy dispersive spectroscopy profile, Mg peak at around 1.3 keV further proves the existence of MgO on the electrode surface. The surface element contents are summarized. It can be found that Mg weight ratio is only 0.47%. The limited Mg amount suggests ALD-derived thin MgO layers onto NCM-10c.

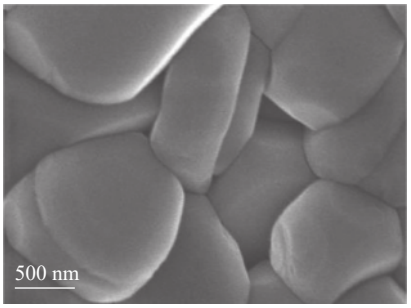

a. The typical SEM image of NCM-0c

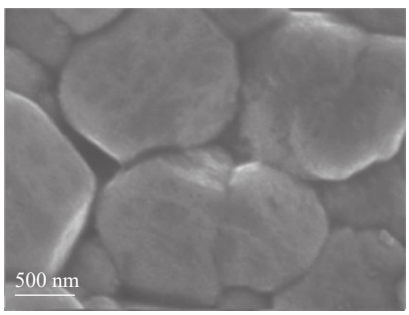

b. The typical SEM image of NCM-2c

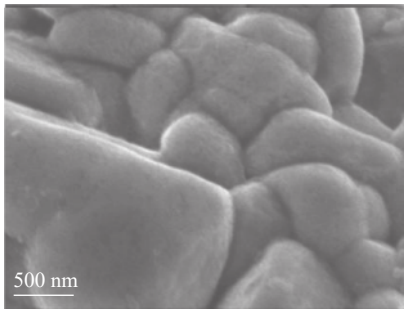

c. The typical SEM image of NCM-5c

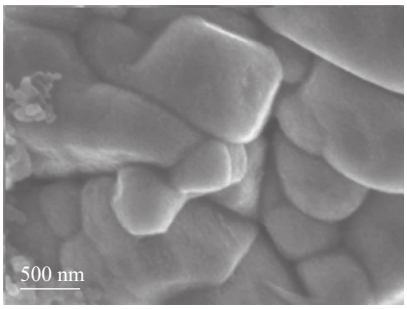

d. The typical SEM image of NCM-10c

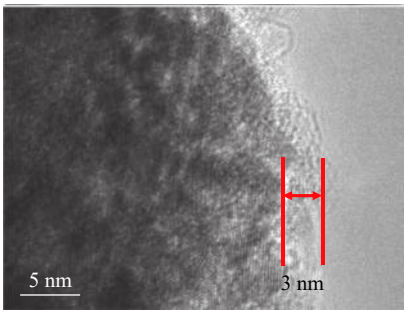

e. HRTEM image of NCM-10c

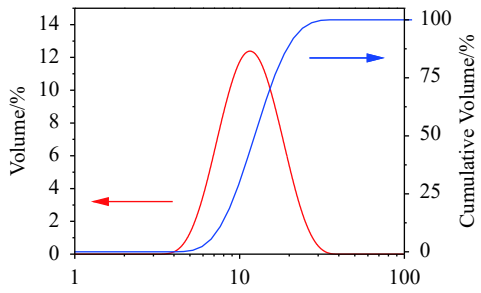

f. The size distribution of NCM-0c

Fig. 1 The typical images and size distribution

The XRD patterns of NCM-0c and NCM-10c are shown in Fig. 2a. Both two patterns are well consistent with the hexagonal α-$NaFeO_2$ layered structure with space group R-3 m. The distinct peaks of (003), (101) and (104) planes are discerned, and no obvious differences can be found by comparing both patterns. This may be attributed to the ultrathin MgO layer exceeding the resolution of XRD. It may also own to the relatively low crystallinity of MgO synthesized at 200 °C. The chemical bonding states of the elements in NCM-10c electrode are characterized by XPS. In Fig. 2b, the strong peaks of C 1s and F 1s are found owing to the existence of the PVDF and acetylene black in the cathode electrodes. As shown in Fig. 2c, the two spin-orbit peaks at 857.5 eV and 878.2 eV are assigned to 2p3/2 and 2p1/2 of Ni in the $LiNi_{0.6}Co_{0.2}Mn_{0.2}O_2$, respectively. And the peaks at 779.7 eV and 795.2 eV correspond to 2p3/2 and 2p1/2 of Co, respectively. Similarly, the spin-orbit peaks of Mn 2p are located at 641.9 eV and 653.5 eV, suggesting the bonding energy of Mn-O in the cathode. Importantly, the signal of Mg 1s is obvious in the spectrum of NCM-10c in Fig. 2f, and the peak at 1 303.1 eV verifies the successful deposition of MgO film.

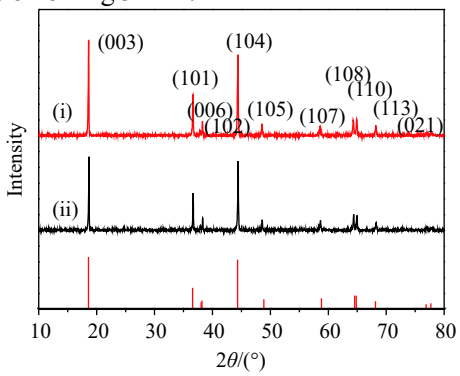

a. XRD patterns of (i) NCM-0c and (ii) NCM-10c

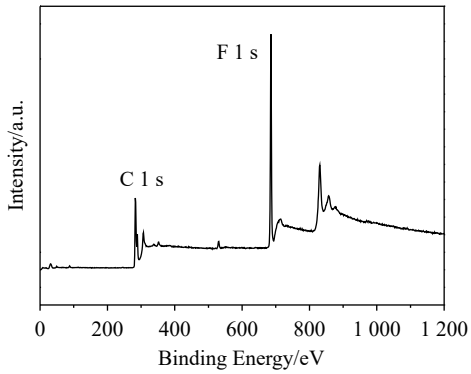

b. XPS spectrum of NCM-10c survey spectrum

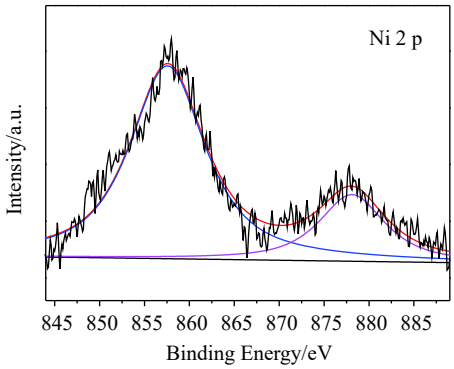

c. XPS spectrum of NCM-10c Ni 2 p

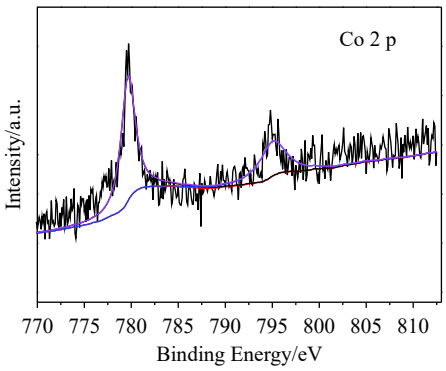

d. XPS spectrum of NCM-10c Co 2 p

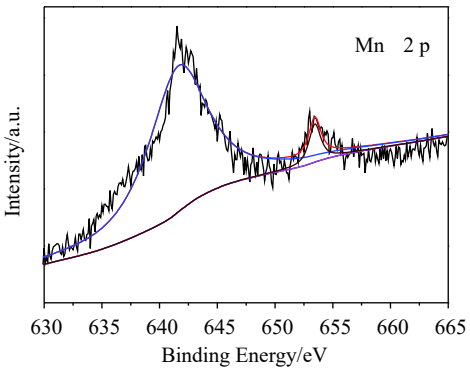

e. XPS spectrum of NCM-10c Mn 2 p

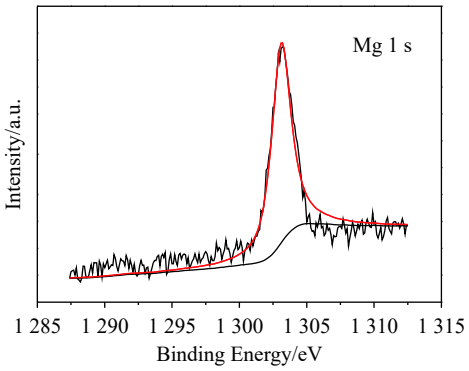

f. XPS spectrum of NCM-10c Mg 1 s

Fig. 2　XRD patterns and XPS spectra of NCM-10c

The CV curves of NCM-0c, NCM-2c, NCM-5c and NCM-10c are expressed in Fig. 3. The peaks in anodic process correspond to the Li^+ extraction from electrodes, while the insertion causes the cathodic peaks[8-9]. With increasing the thicknesses of MgO layer, the positions of the initial anodic peaks shift from 3.89 V to 3.95 V. The polarization is caused by the MgO coating layer with poor conductivity. And this phenomenon can also be found in the following CV curves, for instance, in the 4th cycles the anodic peaks of NCM-0c, NCM-2c, NCM-5c and NCM-10c are located at 3.77 V, 3.78 V, 3.79 V and 3.80 V, respectively. Interestingly, all the electrodes show similar cathodic peak positioned at about 3.69 V. It can be inferred that the MgO coating layer exhibits a weak blocking effect to the lithium ion insertion after the initial cycle.

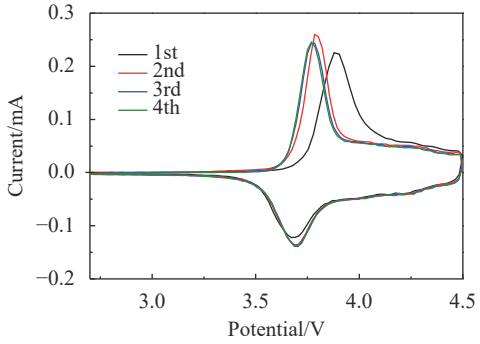

a. The CV curves of NCM-0c

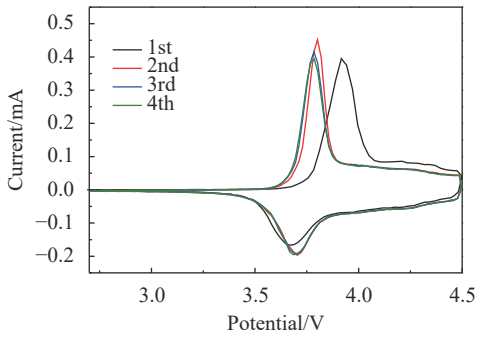

b. The CV curves of NCM-2c

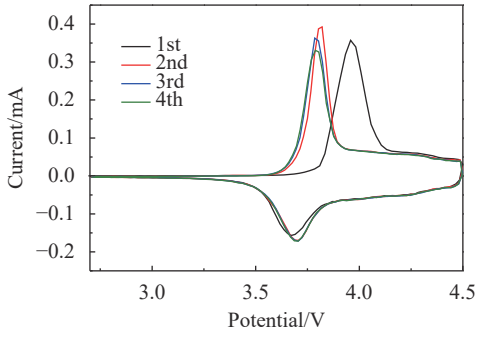

c. The CV curves of NCM-5c

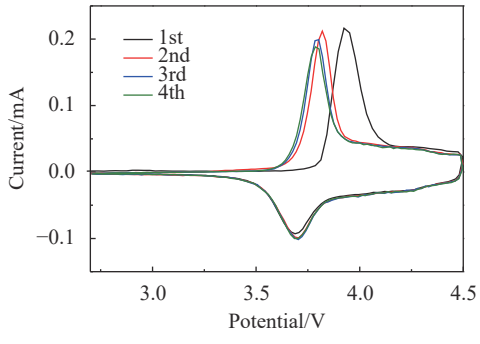

d. The CV curves of NCM-10c

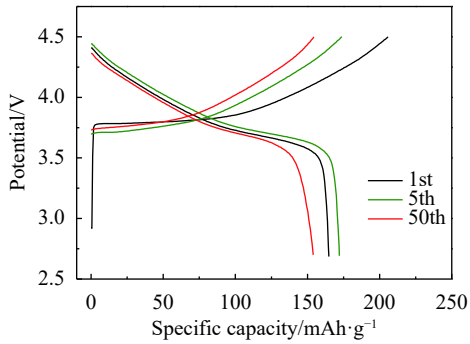

e. The charge-discharge profiles of NCM-0c

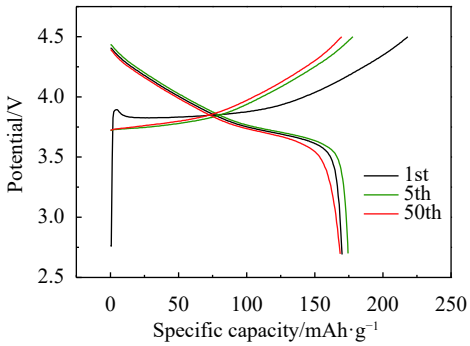

f. The charge-discharge profiles of NCM-2c

Fig. 3 The CV curves and the charge-discharge profiles

The charge-discharge profiles of NCM-0c and NCM-2c in the 1st, 5th, and 50th cycles are summarized in Fig. 3e and 3f. It can be discerned that the specific capacities of NCM-0c show a dramatic degradation during the cycling process, for instance, the charge/discharge capacities decrease from 174/173 mAh·g^{-1} in the 5th cycle to 155/153 mAh·g^{-1} in the 50th cycle. In contrast, the NCM-2c displays good cycling stabilities with high reversible capacities of 177/175 mAh·g^{-1} and 170/169 mAh·g^{-1} at the same test conditions. The initial charge platform of NCM-0c is about 3.75 V in Fig. 3e, while that of NCM-2c is about 3.80 V in Fig. 3f. The polarization is caused by MgO coating layer which is an insulting material to the electron transfer. The discharge platforms of NCM-0c and NCM-2c are 3.71 V, which agrees with the CV curves in Fig. 3a and 3b.

The cycling performances of NCM-0c, NCM-2c, NCM-5c, and NCM-10c are compared at a rate of 1C (224 mA·g^{-1}) in Fig. 4a. The initial charge/discharge specific capacities of NCM-0c, NCM-2c, NCM-5c and NCM-10c are 206.8/164.1 mAh·g^{-1}, 218.2/170 mAh·g^{-1}, 212.3/163.3 mAh·g^{-1} and 268.1/160.1 mAh·g^{-1}, respectively. It can be found that the initial coulombic efficiencies of NCM-0c, NCM-2c and NCM-5c are all about 78%, while NCM-10c expresses a coulombic efficiency of 69%. This suggests the thick MgO coating may be detrimental to the reversibility of cathode electrodes. The NCM-2c shows the highest initial specific capacity among the electrodes. After 100 cycles in the voltage range of 2.7～4.5 V, NCM-2c still exhibits the best capacity retention with a specific capacity of 156.9 mAh·g^{-1}. Meanwhile, that of NCM-0c degrades dramatically from 164.1 mAh·g^{-1} to 131.3 mAh·g^{-1}. As mentioned earlier, the energy density of LIBs can be promoted by increasing the cutoff potentials. To get the performances of $LiNi_{0.6}Co_{0.2}Mn_{0.2}O_2$ with MgO coating layer, the electrodes are also tested in a voltage range from 2.7～4.7 V. And the data are shown in Fig. 4b and 4f. The similar phenomena occur, when the cutoff potential increases to 4.7 V. As expected, the high cutoff potential leads to high specific capacities with low capacity retention. The initial discharge capacity of NCM-2c increases to 200 mAh·g^{-1} from 170 mAh·g^{-1} by rising the cutoff potential from 4.5 V～4.7 V, and a specific capacity of 158 mAh·g^{-1} is obtained after 100 cycles. Similar to the cycling performances at a cutoff potential of 4.5 V, NCM-5c, NCM-10c and NCM-0c successively deliver specific capacities of 151.8 mAh·g^{-1}, 146.9 mAh·g^{-1} and 144 mAh·g^{-1}, respectively.

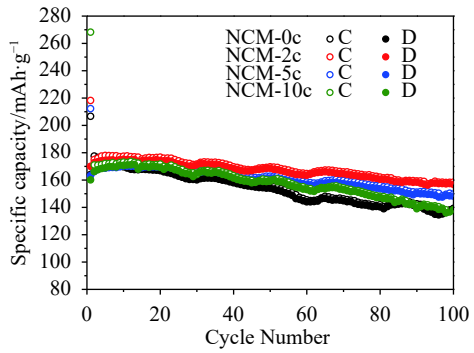

a. Cycling performances in the voltage range of 2.5~4.5 V

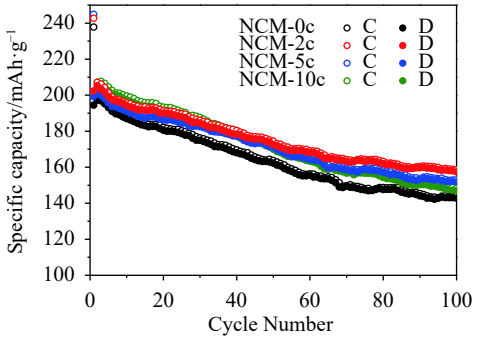

b. Cycling performances in the voltage range of 2.7~4.7 V

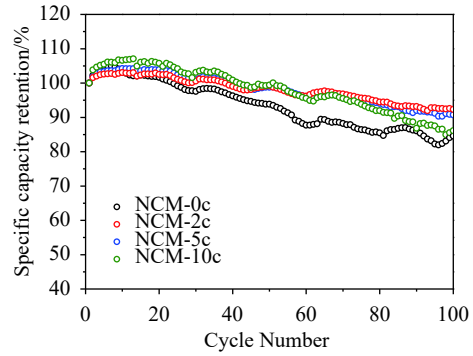

c. Specific capacity retention in the voltage range of 2.7~4.5 V

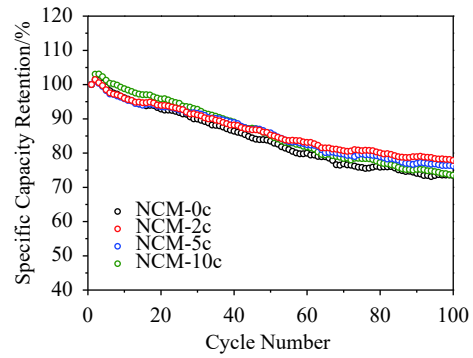

d. Specific capacity retention in the voltage range of 2.7~4.7 V

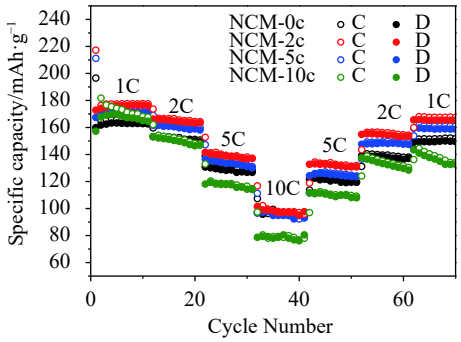

e. Rate capabilities in the voltage range of 2.7~4.5 V

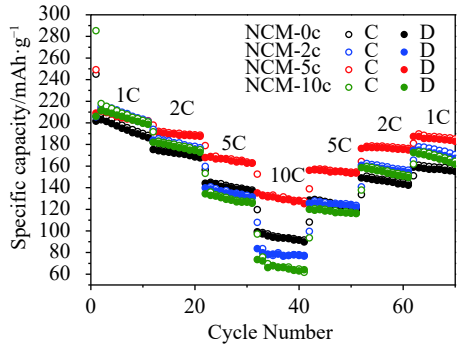

f. Rate capabilities in the voltage range of 2.7~4.7 V

Fig. 4　Cycling performances, specific capacity retention and rate capabilities in different voltage ranges.

As the reflections of electrodes stabilities, capacity retentions are exhibited in Fig. 4c and 4d corresponding to cycling voltage ranges of 2.7～4.5 V and 2.7～4.7 V. In agreement with Fig. 4a, NCM-0c shows the lowest retention among these electrodes in Fig. 4c. After 95 cycles, only 80% of specific capacity is retained in a voltage range of 2.7～ 4.5 V. In comparison, the retention rate of NCM-2c is 93% after 100 cycles. Interestingly, all of electrodes display retention rates higher than 100% in first 20 cycles attributing to the activation process of cathode materials. When the cutoff potential increases to 4.7 V (Fig. 4d), all electrodes show close retention rates. This may be due to severe side-reactions at high potential damaging the surface structure of cathodes. However, after 100 cycles, NCM-2c still shows the highest retention rate. And the high retention rates of NCM-10c in the first 10 cycles verifies a good protection of MgO layer for electrodes.

The rate capabilities of different electrodes in a voltage range of 2.7～ 4.5 V are shown in Fig. 4e. NCM-2c and NCM-5c display higher capacities than NCM-0c at the rates of 1C, 2C and 5C. Notably, after 60 cycles at different current densities, the NCM-2c delivers a capacity of 167 $mAh \cdot g^{-1}$, which is 96% of the specific capacity after 10 cycles at 1C, while the retention rate values of NCM-0c, NCM-5c and NCM-10c are 90%, 92% and 75%, respectively. Moreover, the NCM-10c exhibits the worst performance among these electrodes, especially at high current densities. This may be due to the thick MgO layer with poor conductivity detrimental to the lithium ion transfer. When the electrodes were cycled in the voltage range of 2.7～ 4.7 V, the NCM-2c also shows good rate capability at each current density, especially after cycling at a rate of 10C in Fig. 4f. The reversible capacity of NCM-2c is about 130 $mAh \cdot g^{-1}$ at 10C, while the capacities of the other electrodes are much lower than 100 $mAh \cdot g^{-1}$. After cycling at 1C, 2C, 5C, 10C and 5C, all the electrodes with MgO coating layers exhibit higher specific capacities than NCM-0c. It can be inferred that the MgO coating layers can decrease the corrosion of electrolyte at high rates. Moreover, the rate capabilities of NCM-5c and NCM-10c are worse than NCM-0c at 10C. The similar phenomenon was also reported in the previous work[28].

To investigate the influences of MgO coating layers on the evolution of cathodes, the EIS of NCM-0c and NCM-2c is tested after 5, 10, 20 and 50 cycles. The Nyquist plots of NCM-0c and NCM-2c are shown in Fig. 5a and 5b. The equivalent circuit in Fig. 5d is used to simulate the EIS. The resistance of cell system is represented by R_s, including the electrolyte resistance and various connecting resistances between the different parts in cells. R_{sf} and CPE_{sf} corresponding to the first semicircle of Nyquist in high frequency are used to simulate the resistances in the surface of electrodes. The change of first semicircle in Nyquist can reflect the surface stability of electrodes. R_{ct} and CPE_{ct} represent the resistances caused by charge transfer reactions, which are related to the second semicircle in Nyquist. W_s is attributed to the diffusion process of Li ions in the cathode material, reflecting by the inclined line in low frequency. As seen in Fig. 5a and b, the first Nyquist semicircles of NCM-0c dramatically change with cycles, while those of NCM-2c show a relatively good coincidence. This suggests a better stability of NCM-2c than NCM-0c. The R_{ct} value reflects a stable surface structure and verifies the protection effect of MgO coated on the electrode surface. The fitting R_{ct} results of Nyquist plots are summarized in Fig. 5c. It is obvious that the R_{ct} values of NCM-0c are more than those of NCM-2c after 5, 10, 20 and 50 cycles. Furthermore, the R_{ct} of NCM-2c is more stable than that of NCM-0c. Especially, after 5 cycles, R_{ct} of NCM-0c is close to 150 Ω, while the R_{ct} of NCM-2c is only 75 Ω. These are good evidences to prove that the cathode structure is stabilized by the MgO coating layers.

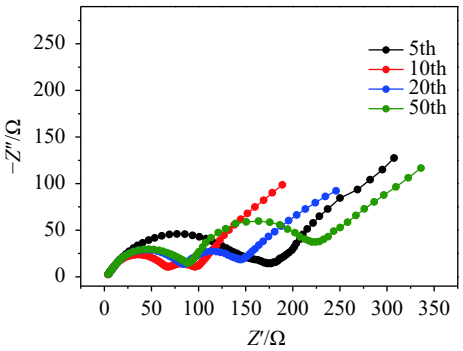

a. Nyquist plots of NCM-0c

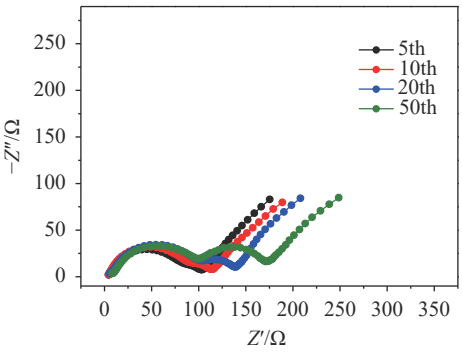

b. Nyquist plots of NCM-2c

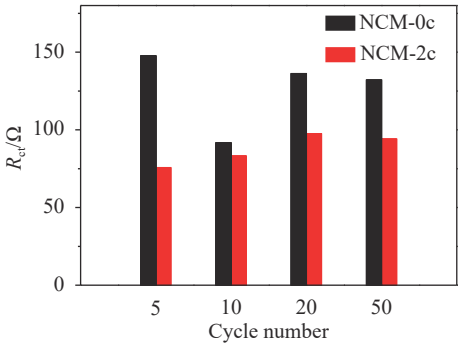

c. The fitted parameters of charge transfer resistance (Rct) after 5, 10, 20 and 50 cycles

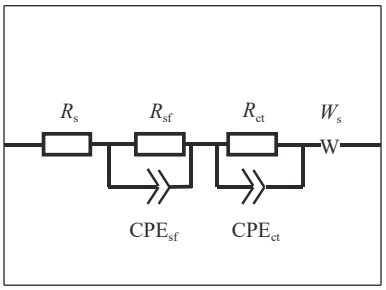

d. The equivalent circuit used to simulate electrode reactions

Fig. 5 Electrochemical impedance spectroscopy of NCM-0c and NCM-2c

3 Conclusion

In this study, for the first time, the electrochemical performances of $LiNi_{0.6}Co_{0.2}Mn_{0.2}O_2$ material were improved by depositing ultrathin MgO layers onto electrodes. By preciously controlling the MgO thickness, it was found that 2 –ALD- cycle deposition of MgO on $LiNi_{0.6}Co_{0.2}Mn_{0.2}O_2$ electrodes can efficiently promote the cycling performance and rate capability. The electrochemical performance promotion owns to the stabilization and protection effects of ALD derived ultrathin MgO coating layer. Our results exhibit the potential of ALD derived MgO for improvement of cathode performance for LIBs.

4 Acknowledgments

This research was supported by Academic Innovation Funding of Tianjin Normal University (52XC1404) and Training Plan of Leader Talent of University in Tianjin.

References

[1] LI X, LIU J, BANIS M N, et al. Atomic layer deposition of solid-state electrolyte coated cathode materials with superior high-voltage cycling behavior for lithium ion battery application[J]. Energy & Environmental Science, 2014, 7(2): 768-778.

[2] WU H, WANG Z, LIU S, et al. Fabrication of Li^+-conductive Li_2ZrO_3-based shell encapsulated $LiNi_{0.5}Co_{0.2}Mn_{0.3}O_2$ microspheres as high-rate and long-life cathode materials for Li-ion batteries[J]. ChemElectroChem, 2015, 2(12): 1921-1928.

[3] JUNG S K, GWON H, HONG J, et al. Understanding the degradation mechanisms of $LiNi_{0.5}Co_{0.2}Mn_{0.3}O_2$ cathode material in lithium ion batteries[J]. Advanced Energy Materials, 2014, 4(1): 1300787.

[4] WANG Z, LIU E, HE C, et al. Effect of amorphous $FePO_4$ coating on structure and electrochemical performance of $Li_{1.2}Ni_{0.13}Co_{0.13}Mn_{0.54}O_2$ as cathode material for Li-ion batteries[J]. Journal of Power Sources, 2013, 236: 25-32.

[5] JU S H, KANG I S, LEE Y S, et al. Improvement of the cycling performance of $LiNi_{0.6}Co_{0.2}Mn_{0.2}O_2$ cathode active materials by a dual-conductive polymer coating[J]. ACS Applied Materials & Interfaces, 2014, 6(4): 2546-2552.

[6] KIM NY, YIM T, SONG J H, et al. Microstructural study on degradation mechanism of layered $LiNi_{0.6}Co_{0.2}Mn_{0.2}O_2$ cathode materials by analytical transmission electron microscopy[J]. Journal of Power Sources, 2016, 307: 641-648.

[7] CHEN Y, ZHANG Y, WANG F, et al. Improve the structure and electrochemical performance of $LiNi_{0.6}Co_{0.2}Mn_{0.2}O_2$ cathode material by nano-Al_2O_3 ultrasonic coating[J]. Journal of Alloys and Compounds, 2014, 611: 135-141.

[8] WANG H, GE W, LI W, et al. Facile fabrication of ethoxy-functional polysiloxane wrapped $LiNi_{0.6}Co_{0.2}Mn_{0.2}O_2$ cathode with improved cycling performance for rechargeable Li-ion battery[J]. ACS Applied Materials & Interfaces, 2016, 8(28): 18439-18449.

[9] CHENG K L, MU D B, WU B R, et al. Electrochemical performance of a nickel-rich $LiNi_{0.6}Co_{0.2}Mn_{0.2}O_2$ cathode material for lithium-ion batteries under different cut-off voltages[J]. International Journal of Minerals, Metallurgy, and Materials, 2017, 24(3): 342-351.

[10] ZHENG H, SUN Q, LIU G, et al. Correlation between dissolution behavior and electrochemical cycling performance for $LiNi_{1/3}Co_{1/3}Mn_{1/3}O_2$-based cells[J]. Journal of Power Sources, 2012, 207: 134-140.

[11] KLEINER K, EHRENBERG H. Challenges considering the degradation of cell components in commercial lithium-ion cells: A review and evaluation of present systems[J]. Topics in Current Chemistry, 2017, 375(3): 54.

[12] MYUNG S T, MAGLIA F, PARK K, et al. Nickel-rich layered cathode materials for automotive lithium-ion batteries: achievements and perspectives[J]. ACS Energy Letters, 2017, 2(1): 196-223.

[13] KANG S H, KIM J, STOLL M E, et al. Layered $Li(Ni_{0.5-x}Mn_{0.5-x}M'_{2x})O_2$ (M′=Co, Al, Ti; x=0, 0.025) cathode materials for Li-ion rechargeable batteries[J]. Journal of Power Sources, 2002, 112(1): 41-48.

[14] CHEN C H, LIU J, STOLL M E, et al. Aluminum-doped lithium nickel cobalt oxide electrodes for high-power lithium-ion batteries[J]. Journal of Power Sources, 2004, 128(2): 278-285.

[15] NAYAK P K, GRINBLAT J, LEVI M, et al. Al doping for mitigating the capacity fading and voltage decay of layered Li and Mn-rich cathodes for Li-ion batteries[J]. Advanced Energy Materials, 2016, 6(8): 1502398.

[16] LUO Y, LU T, ZHANG Y, et al. Surface-segregated, high-voltage spinel lithium-ion battery cathode material $LiNi_{0.5}Mn_{1.5}O_4$ cathodes by aluminium doping with improved high-rate cyclability[J]. Journal of Alloys and Compounds, 2017, 703: 289-297.

[17] LIU X, LI D, MO Q, et al. Facile synthesis of aluminum-doped $LiNi_{0.5}Mn_{1.5}O_4$ hollow microspheres and their electrochemical performance for high-voltage Li-ion batteries[J]. Journal of Alloys and Compounds, 2014, 609: 54-59.

[18] MIAO X, NI H, ZHANG H, et al. Li_2ZrO_3-coated$_{0.4}Li_2MnO_3\cdot 0.6LiNi_{1/3}Co_{1/3}Mn_{1/3}O_2$ for high performance cathode material in lithium-ion battery[J]. Journal of Power Sources, 2014, 264: 147-154.

[19] CHEN J, LI Z, XIANG H, et al. Enhanced electrochemical performance and thermal stability of a $CePO_4$-coated $Li_{1.2}Ni_{0.13}Co_{0.13}Mn_{0.54}O_2$ cathode material for lithium-ion batteries[J]. RSC Advances, 2015, 5(4): 3031-3038.

[20] FU F, XU G L, WANG Q, et al. Synthesis of single crystalline hexagonal nanobricks of $LiNi_{1/3}Co_{1/3}Mn_{1/3}O_2$ with high percentage of exposed {010} active facets as high rate performance cathode material for lithium-ion battery[J]. Journal of Materials Chemistry A, 2013, 1(12): 3860-3864.

[21] LIN F, MARKUS I M, NORDLUND D, et al. Surface reconstruction and chemical evolution of stoichiometric layered cathode materials for lithium-ion batteries[J]. Nature Communications, 2014, 5: 3529.

[22] YAN P, NIE A, ZHENG J, et al. Evolution of lattice structure and chemical composition of the surface reconstruction layer in $Li_{1.2}Ni_{0.2}Mn_{0.6}O_2$ cathode material for lithium ion batteries[J]. Nano Letters, 2014, 15(1): 514-522.

[23] NAN C, LU J, LI L, et al. Size and shape control of $LiFePO_4$ nanocrystals for better lithium ion battery cathode materials[J]. Nano Research, 2013, 6(7): 469-477.

[24] MIAO X, YAN Y, WANG C, et al. Optimal microwave-assisted hydrothermal synthesis of nanosized $xLi_2MnO_3\cdot(1-x)$ $LiNi_{1/3}Co_{1/3}Mn_{1/3}O_2$ cathode materials for lithium ion battery[J]. Journal of Power Sources, 2014, 247: 219-227.

[25] XIANG X, LI X, LI W. Preparation and characterization of size-uniform $Li[Li_{0.131}Ni_{0.304}Mn_{0.565}]O_2$ particles as cathode materials for high energy lithium ion battery[J]. Journal of Power Sources, 2013, 230: 89-95.
[26] LAI F, ZHANG X, WANG H, et al. Three-dimension hierarchical Al_2O_3 nanosheets wrapped $LiMn_2O_4$ with enhanced cycling stability as cathode material for lithium ion batteries[J]. ACS Applied Materials & Interfaces, 2016, 8(33): 21656-21665.
[27] CHO J, KIM Y J, PARK B. Novel $LiCoO_2$ cathode material with Al_2O_3 coating for a Li ion cell[J]. Chemistry of Materials, 2000, 12(12): 3788-3791.
[28] LI X, LIU J, MENG X, et al. Significant impact on cathode performance of lithium-ion batteries by precisely controlled metal oxide nanocoatings via atomic layer deposition[J]. Journal of Power Sources, 2014, 247: 57-69.
[29] LEE Y S, SHIN W K, KANNAN A G, et al. Improvement of the cycling performance and thermal stability of lithium-ion cells by double-layer coating of cathode materials with Al_2O_3 nanoparticles and conductive polymer[J]. ACS Applied Materials & Interfaces, 2015, 7(25): 13944-13951.
[30] WALLER G H, BROOKE P D, RAINWATER B H, et al. Structure and surface chemistry of Al_2O_3 coated $LiMn_2O_4$ nanostructured electrodes with improved lifetime[J]. Journal of Power Sources, 2016, 306: 162-170.
[31] NOBILI F, CROCE F, TOSSICI R, et al. Sol-gel synthesis and electrochemical characterization of Mg-/Zr-doped $LiCoO_2$ cathodes for Li-ion batteries[J]. Journal of Power Sources, 2012, 197: 276-284.
[32] GNANARAJ J S, POL V G, GEDANKEN A, et al. Improving the high-temperature performance of $LiMn_2O_4$ spinel electrodes by coating the active mass with MgO via a sonochemical method[J]. Electrochemistry Communications, 2003, 5(11): 940-945.
[33] WANG D, HUANG Y, HUO Z, et al. Synthesize and electrochemical characterization of Mg-doped Li-rich layered $Li[Li_{0.2}Ni_{0.2}Mn_{0.6}]O_2$ cathode material[J]. Electrochimica Acta, 2013, 107: 461-466.
[34] MLADENOV M, STOYANOVA R, ZHECHEVA E, et al. Effect of Mg doping and MgO-surface modification on the cycling stability of $LiCoO_2$ electrodes[J]. Electrochemistry Communications, 2001, 3(8): 410-416.
[35] SHI S J, TU J P, TANG Y Y, et al. Enhanced cycling stability of $Li[Li_{0.2}Mn_{0.54}Ni_{0.13}Co_{0.13}]O_2$ by surface modification of MgO with melting impregnation method[J]. Electrochimica Acta, 2013, 88: 671-679.
[36] ZHANG Z, GONG Z, YANG Y. Electrochemical performance and surface properties of bare and TiO_2-coated cathode materials in lithium-ion batteries[J]. The Journal of Physical Chemistry B, 2004, 108(45): 17546-17552.
[37] ZHENG J M, LI J, ZHANG Z R, et al. The effects of TiO_2 coating on the electrochemical performance of $Li[Li_{0.2}Mn_{0.54}Ni_{0.13}Co_{0.13}]O_2$ cathode material for lithium-ion battery[J]. Solid State Ionics, 2008, 179(27-32): 1794-1799.
[38] ZHANG X, BELHAROUAK I, LI L, et al. Structural and electrochemical study of $A_{l2}O_3$ and TiO_2 coated $Li_{1.2}Ni_{0.13}Mn_{0.54}Co_{0.13}O_2$ cathode material using ALD[J]. Advanced Energy Materials, 2013, 3(10): 1299-1307.
[39] SCLAR H, HAIK O, MENACHEM T, et al. The effect of ZnO and MgO coatings by a sono-chemical method, on the stability of $LiMn_{1.5}Ni_{0.5}O_4$ as a cathode material for 5 V Li-ion batteries[J]. Journal of the Electrochemical Society, 2012, 159(3): A228-A237.
[40] TU J, ZHAO XB, XIE J, et al. Enhanced low voltage cycling stability of $LiMn_2O_4$ cathode by ZnO coating for lithium ion batteries[J]. Journal of Alloys and Compounds, 2007, 432(1-2): 313-317.
[41] CHANG W, CHOI J W, IM J C, et al. Effects of ZnO coating on electrochemical performance and thermal stability of $LiCoO_2$ as cathode material for lithium-ion batteries[J]. Journal of Power Sources, 2010, 195(1): 320-326.
[42] SHIM J H, LEE S, PARK S S. Effects of MgO coating on the structural and electrochemical characteristics of $LiCoO_2$ as cathode materials for lithium ion battery[J]. Chemistry of Materials, 2014, 26(8): 2537-2543.
[43] WANG Z, HUANG X, CHEN L. Performance improvement of surface-modified $LiCoO_2$ cathode materials: an infrared absorption and X-Ray photoelectron spectroscopic investigation[J]. Journal of the Electrochemical Society, 2003, 150(2): 199-208.
[44] WANG Z, WU C, LIU L, et al. Electrochemical evaluation and structural characterization of commercial $LiCoO_2$ surfaces modified with MgO for lithium-ion batteries[J]. Journal of the Electrochemical Society, 2002, 149(4): 466-471.
[45] GUAN C, WANG J. Recent development of advanced electrode materials by atomic layer deposition for electrochemical energy storage[J]. Advanced Science, 2016, 3: 1500405.
[46] WOO J H, TRAVIS J J, GEORGE S M, et al. Utilization of Al_2O_3 atomic layer deposition for Li ion pathways in solid state li batteries[J]. Journal of the Electrochemical Society, 2015, 162(3): 344-349.
[47] YU M, MA J, SONG H, et al. Atomic layer deposited TiO_2 on a nitrogen-doped graphene/sulfur electrode for high performance lithium-sulfur batteries[J]. Energy & Environmental Science, 2016, 9(4): 1495-1503.
[48] LI X, LIU J, WANG B, et al. Nanoscale stabilization of Li-sulfur batteries by atomic layer deposited Al_2O_3[J]. RSC Advances, 2014, 4(52): 27126-27129.
[49] YAN B, LI X, BAI Z, et al. A review of atomic layer deposition providing high performance lithium sulfur batteries[J]. Journal of Power Sources, 2017, 338: 34-48.
[50] KOU H, LI X, SHAN H, et al. An optimized Al_2O_3 layer for enhancing the anode performance of $NiCo_2O_4$ nanosheets for sodium-ion batteries[J]. Journal of Materials Chemistry A, 2017, 5(34): 17881-17888.
[51] LI X, MENG X, LIU J, et al. Tin oxide with controlled morphology and crystallinity by atomic layer deposition onto graphene nanosheets for enhanced lithium storage[J]. Advanced Functional Materials, 2012, 22(8): 1647-1654.

编 辑 刘飞阳